ACS Energy LETTERS

Cite This: ACS Energy Lett. 2018, 3, 2527−2532

http://pubs.acs.org/journal/aelccp

LETTER

High-Performance Electrochemical CO_2 Reduction Cells Based on Non-noble Metal Catalysts

Xu Lu,[†,‡,▽] Yueshen Wu,[†,‡,▽] Xiaolei Yuan,[†,‡,§] Ling Huang,[†,‡,∥] Zishan Wu,[†,‡] Jin Xuan,[⊥] Yifei Wang,[#] and Hailiang Wang*[,†,‡]

[†]Department of Chemistry, Yale University, New Haven, Connecticut 06520, United States

[‡]Energy Sciences Institute, Yale University, West Haven, Connecticut 06516, United States

[§]Institute of Functional Nano and Soft Materials (FUNSOM), Jiangsu Key Laboratory for Carbon-Based Functional Materials and Devices, Soochow University, Suzhou 215000, China

[∥]Department of Advanced Energy Materials, Sichuan University, Chengdu 610065, China

[⊥]Department of Chemical Engineering, Loughborough University, Loughborough LE11 3TU, United Kingdom

[#]Department of Mechanical Engineering, University of Hong Kong, Hong Kong, China

Supporting Information

ABSTRACT: The promise and challenge of electrochemical mitigation of CO_2 calls for innovations on both catalyst and reactor levels. In this work, enabled by our high-performance and earth-abundant CO_2 electroreduction catalyst materials, we developed alkaline microflow electrolytic cells for energy-efficient, selective, fast, and durable CO_2 conversion to CO and $HCOO^-$. With a cobalt phthalocyanine-based cathode catalyst, the CO-selective cell starts to operate at a 0.26 V overpotential and reaches a Faradaic efficiency of 94% and a partial current density of 31 mA/cm^2 at a 0.56 V overpotential. With a SnO_2-based cathode catalyst, the $HCOO^-$-selective cell starts to operate at a 0.76 V overpotential and reaches a Faradaic efficiency of 82% and a partial current density of 113 mA/cm^2 at a 1.36 V overpotential. In contrast to previous studies, we found that the overpotential reduction from using the alkaline electrolyte is mostly contributed by a pH gradient near the cathode surface.

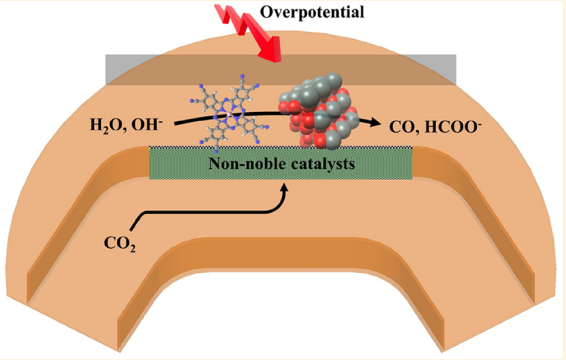

Electrochemical conversion of CO_2 offers a promising solution to offset the greenhouse gas and ocean acidification issues. This process is particularly appealing when the transformation of concentrated carbon emissions into fuels or chemical feedstocks is driven by excess electricity generated from renewable sources.[1−3] Among various CO_2 reduction reaction (CO_2RR) options, formate ($HCOO^-$) synthesis is one of the most viable technology pathways as the cost could be levelized to $0.46/kg, below the commercial formic acid price threshold.[4] CO production, if coupled with the Fischer−Tropsch process, is also plausible with the potential to produce diesel fuel at the cost of $4.4/gallon per gas equivalent.[1,4] More reduced products, such as ethanol, are limited by a minimum cost of $8.2/gallon per gas equivalent, lacking technoeconomic feasibility.[4] However, $HCOO^-$ synthesis and CO production are still hindered by inefficient kinetics. From this perspective, designing active, selective, durable and low-cost CO_2RR catalysts is the key. Meanwhile, to push CO_2RR toward a higher level of industrial relevance, it is important to improve the full-cell performance by developing reactors with enhanced mass transport and reduced internal resistance.

Extensive effort has been devoted to the search for efficient CO_2RR catalyst materials. Some noble metals are both active and selective, such as Au for CO_2-to-CO conversion[5−7] and Pd for HCOOH generation.[8,9] However, their high cost and low catalytic stability are less suitable for practical electrochemical reactors. Cu-based catalysts have displayed a wide product spectrum covering CO,[10] CH_4,[11,12] C_2H_4,[13,14] $HCOO^-$,[15] and multicarbon species.[11,16] Yet, high selectivity and long-term stability are still not easy to achieve.[17] SnO_x is able to reduce CO_2 to $HCOO^-$ with high Faradaic efficiency (FE) and good

Received: September 7, 2018
Accepted: September 18, 2018
Published: September 18, 2018

DOI: 10.1021/acsenergylett.8b01681
ACS Energy Lett. 2018, 3, 2527−2532

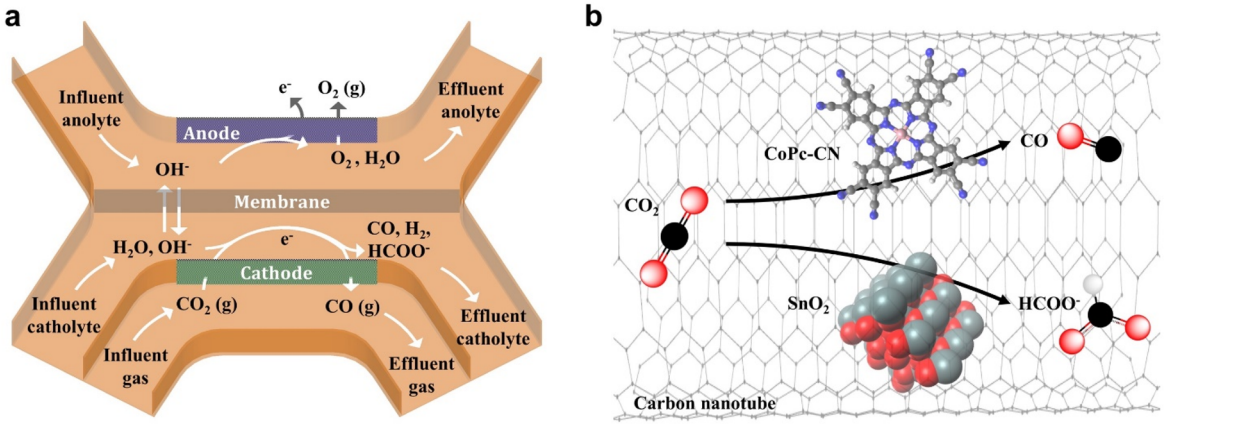

Figure 1. (a) Gas and liquid flows and electrochemical reactions in the flow cell. (b) CoPc-CN molecules and SnO_2 nanoparticles supported on CNTs as cathode electrocatalysts for CO_2 conversion to CO and $HCOO^-$, respectively.

stability,[18] and it has been reported that its catalytic performance can be improved by hybridizing with a Cu[19,20] or Ag[21] component. For CO_2-to-CO conversion, we have recently developed a hybrid material with molecularly structured catalytic sites, namely, cyano-substituted cobalt phthalocyanine molecules (CoPc-CN) anchored on carbon nanotubes (CNTs), which demonstrates high selectivity, large geometric current density, and high turnover frequency at a relatively low overpotential.[22]

In the pursuit of electrochemical reactors for CO_2 reduction, the majority of reported studies have been based on two-compartment H-shape cells.[23,24] A cell voltage above 3 V is typically required to reach a moderate current density of 6 mA/cm^2.[23,24] Typical H cells are also subject to low maximum reaction rates limited by mass transport because of the relatively large thickness of boundary layers.[25] Introducing a membrane electrode assembly was effective in reducing the distance between the two electrodes, but at the cost of either a high catalyst loading or a low product yield.[26,27] The effects of ionomers in MEA cells remain to be fully understood.[28] Adopting flow cells with gas diffusion electrodes (GDEs) was able to further improve the device performance[29−33] and should also in theory be able to separate more clearly the effects of electrolyte composition on mass transport versus reaction kinetics in comparison to the H-cell design,[34−36] although researchers have not fully understood the three-phase interface. In particular, Kenis et al. achieved a current density of 135 mA/cm^2 and a FE_{CO} of 95% at a cell voltage of 2.5 V in spite of the voltage loss caused by the relatively large interelectrode distance, based on Ag nanoparticles as the cathode catalyst and a 1 M KOH aqueous solution as the electrolyte. This strategy[29] was also extended to other noble metal catalysts.[30−32] The onset cell voltage reduction from using the alkaline electrolyte was first explained by destabilization of the $CO_2^{\bullet-}$ intermediate by specific anions absorbed on the Ag surface[29] and in a later study attributed to the non-proton-coupled rate-determining electron-transfer step on Au surface.[33] The latter explanation would make sense if CO_2 does not react with KOH on the cathode and alter the pH near the catalyst surface, which remains to be verified by experimentally probing the local pH.

Here we report electrochemical flow cells equipped with catalysts based on earth-abundant elements that can perform selective and efficient CO_2 reduction to CO or $HCOO^-$. With CoPc-CN/CNT as the cathode catalyst and CoO_x/CNT as the anode catalyst, our cell starts to split CO_2 into CO and O_2 at a full-cell voltage of 1.6 V, corresponding to a nominal cell overpotential (i.e., η_{cell}) of 0.26 V. The peak FE_{CO} of 94% is reached at η_{cell} = 0.56 V and a partial current density (i.e., j_{CO}) of 31 mA/cm^2. j_{CO} exceeds 80 mA/cm^2 at η_{cell} = 0.96 V. With SnO_2/CNT as the cathode catalyst, conversion of CO_2 and H_2O to $HCOO^-$ and O_2 occurs at a full-cell voltage of 1.9 V, corresponding to a η_{cell} of 0.76 V. The FE_{HCOO^-} reaches 82% at η_{cell} = 1.36 V and j_{HCOO^-} = 113 mA/cm^2. The j_{HCOO^-} approaches 200 mA/cm^2 at η_{cell} = 1.76 V. Our devices represent the most efficient non-noble metal catalyst-based electrolytic cells that have been reported to date for reducing CO_2 to CO or $HCOO^-$. Further analysis attributes the high electrochemical performance to our active, selective, and durable CO_2RR catalysts; to the low internal resistance and enhanced mass transport of the microflow cell; and importantly, to a pH gradient created by the neutralization of OH^- by CO_2 near the cathode surface.

The core component of our CO_2 electroreduction system (Figure S1) is a microflow cell that facilitates two laminar electrolyte fluids (i.e., anolyte and catholyte) and a CO_2 gas stream to flow in parallel along microscale channels (Figure 1). We note that gaseous products (CO or H_2) could be mixed in either the CO_2 gas stream or the liquid catholyte, which was not explicitly discussed in the previous studies on similar cells. To ensure accurate product quantification, we invented a gas-tight collector, into which both the gas and electrolyte effluents were driven (Figure S1). All the gaseous products could therefore be collected for online gas chromatograph sampling. The effectiveness of this design was vindicated by near-unity total FEs. The functionality of the microflow cell was first verified by using Au nanoparticles (Figure S2) as the cathode catalyst for CO_2RR, CoO_x/CNT (Figure S3) as the anode catalyst for the O_2 evolution reaction (OER), and a 0.5 M $KHCO_3$ aqueous solution as the electrolyte. The Au cathode demonstrated electrocatalytic performance in the flow cell (Figure S4) comparable with that in a prevalent three-electrode H cell (Figure S2) over a wide cathode potential range.

Our CO-producing cell employs CoPc-CN/CNT (Figure S5) as the cathode catalyst and CoO_x/CNT as the anode catalyst in a 1 M KOH aqueous electrolyte. Significant CO generation could be observed at a full-cell voltage as low as 1.6 V (Figure 2a), which corresponds to a η_{cell} of 0.26 V and represents one of the lowest that have been reported for electrochemical CO_2 conversion to CO (Table S1). As the cell voltage was increased, CO production became more substantial. At a cell voltage of

DOI: 10.1021/acsenergylett.8b01681
ACS Energy Lett. 2018, 3, 2527−2532

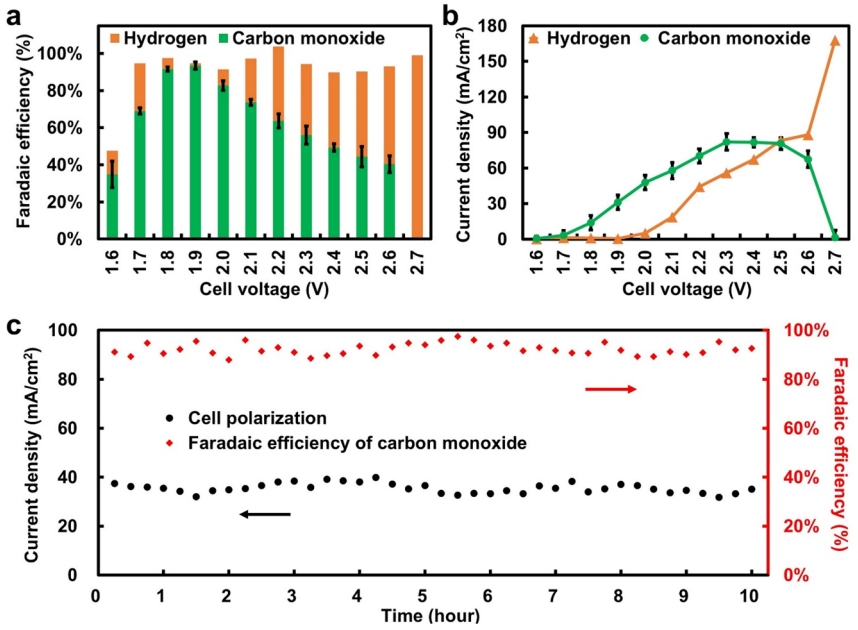

Figure 2. (a) Faradaic efficiencies and (b) partial current densities for CO and H_2 vs the voltage of the electrolytic cell with CoPc-CN/CNT as the cathode catalyst, CoO_x/CNT as the anode catalyst, and 1 M KOH as the electrolyte. (c) Total current density and Faradaic efficiency for CO production during a 10 h operation at a constant cell voltage of 2.0 V. Error bars represent the standard deviations from multiple measurements.

1.9 V (i.e., η_{cell} = 0.56 V), FE_{CO} reached 94% with j_{CO} = 31 mA/cm^2 (Figure 2b). As the cell voltage was further elevated, CO selectivity decreased, whereas j_{CO} continued to increase, reaching a maximum of 82 mA/cm^2 at a cell voltage of 2.3 V. j_{H_2} also increased with the cell voltage. At 2.7 V, H_2 became the dominant product with j_{H_2} = 168 mA/cm^2 while FE_{CO} dramatically dropped to 0.9% with j_{CO} = 1.5 mA/cm^2. The general dependence of product distribution on potential is consistent with that measured for the same cathode catalyst in a three-electrode H cell (Figure S5). A long-term operation was carried out for 10 h at a constant cell voltage of 2.0 V (i.e., η_{cell} = 0.66 V), with the catholyte and anolyte being circulated separately. In spite of fluctuations due to gaseous bubble invasion and microflow disturbance, j_{total} stayed between 35 and 40 mA/cm^2 and FE_{CO} was stable around 90% throughout the entire period (Figure 2c). Stability at high performance as such has been reported only for an alkaline flow cell operating with a noble Au catalyst.[33]

We then steered the system to $HCOO^-$ production by switching the cathode catalyst to SnO_2/CNT (Figure S6). Significant $HCOO^-$ production could be detected at a cell voltage of 1.9 V (Figure 3a), corresponding to a η_{cell} of 0.76 V. FE_{HCOO^-} increased with the applied cell voltage, reaching a maximum of 82% at a j_{HCOO^-} of 113 mA/cm^2 and a cell voltage of 2.5 V (i.e., η_{cell} = 1.36 V). The high FE_{HCOO^-} of 80% was retained until the cell voltage was increased to 2.9 V, where j_{HCOO^-} approached 200 mA/cm^2 (Figure 3b). This performance is close to industry-relevant levels[37] and outperforms some of the most efficient CO_2-to-$HCOO^-$ electrolytic devices reported to date (Table S1).[38−40] Under the electrolyte circulation mode, the cell was operated at a constant cell voltage of 2.3 V (i.e., η_{cell} = 1.16 V) for 35 h (Figure 3c). The entire electrolysis yielded 0.7 M of $HCOO^-$ in the 12 mL electrolyte, with FE_{HCOO^-} between 60% and 70% and the total current density between 30 and 50 mA/cm^2. The decay in selectivity and current density during the long-term electrolysis could be attributed to the consumption of OH^- on the anode side and hence the gradual decrease in the pH of the anolyte. A lower pH on the anode side could worsen the OER kinetics and decrease the full-cell performance. While the pH of the catholyte is also expected to change, the local pH near the cathode catalyst surface is likely held stable by the chemical reaction between CO_2 and KOH, which will be discussed below.

The high electrochemical performance is due to both the catalysts and the cell design. The CoPc-CN/CNT and SnO_2/CNT, with high catalytic selectivity, activity, and durability, ensure the efficient conversion of CO_2 to CO and $HCOO^-$, respectively. The microflow cell architecture effectively minimizes the distance between the cathode and anode and thus reduces the internal resistance (estimated to be 0.153 Ω/cm^2). The GDE provides a three-phase interface for the electrochemical reactions to occur. The effective slip velocities at the GDE−CO_2 and GDE−electrolyte interfaces, in association with the parallel drift velocity profile near the electrode surface, reduce the diffusion boundary layer thickness and enhance the convective/diffusive mass transport. More essentially, the KOH electrolyte plays an indispensable role. In a control experiment using Au as the cathode catalyst and CoO_x/CNT as the anode catalyst, we found that the cell requires a 470 mV higher overpotential to reach a current density of 20 mA/cm^2 when operating in a neutral 0.5 M $KHCO_3$ electrolyte compared to that in the basic 1 M KOH electrolyte (Figures 4, S4, and S7). The same situation occurs when using CoPc-CN/CNT (Figures 2, 4, and S8) or SnO_2/CNT (Figure 3, 4, and S9) as the cathode catalyst. While the voltage gain for the KOH cell can be partially explained by the presumption that the OER is more efficient in alkaline than in neutral electrolyte,[41,42] there may be other important contributors to the observed performance improvement.

In another Au-based control experiment, we compared the KOH cell with a $KHCO_3$ (catholyte)−KOH (anolyte) dual-electrolyte cell. These two cells exhibited very similar

DOI: 10.1021/acsenergylett.8b01681
ACS Energy Lett. 2018, 3, 2527−2532

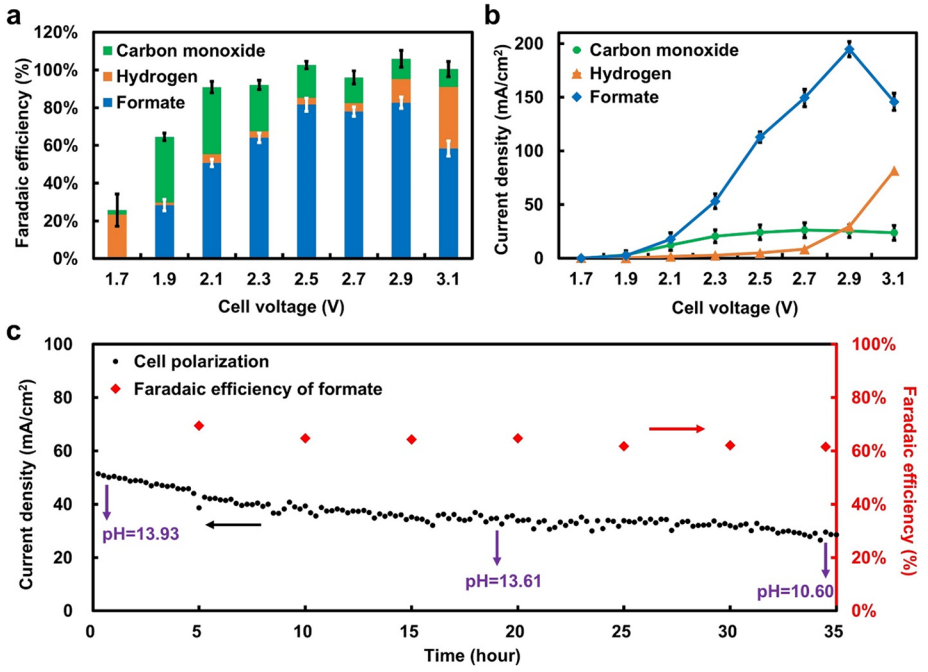

Figure 3. (a) Faradaic efficiencies and (b) partial current densities for $HCOO^-$, CO, and H_2 vs the voltage of the electrolytic cell with SnO_2/CNT as the cathode catalyst, CoO_x/CNT as the anode catalyst, and 1 M KOH as the electrolyte. (c) Total current density and Faradaic efficiency for $HCOO^-$ production during a 35 h operation at a constant cell voltage of 2.3 V. The catholyte was sampled for pH measurements at the 0th, 18th, and 35th hour. Error bars represent the standard deviations from multiple measurements.

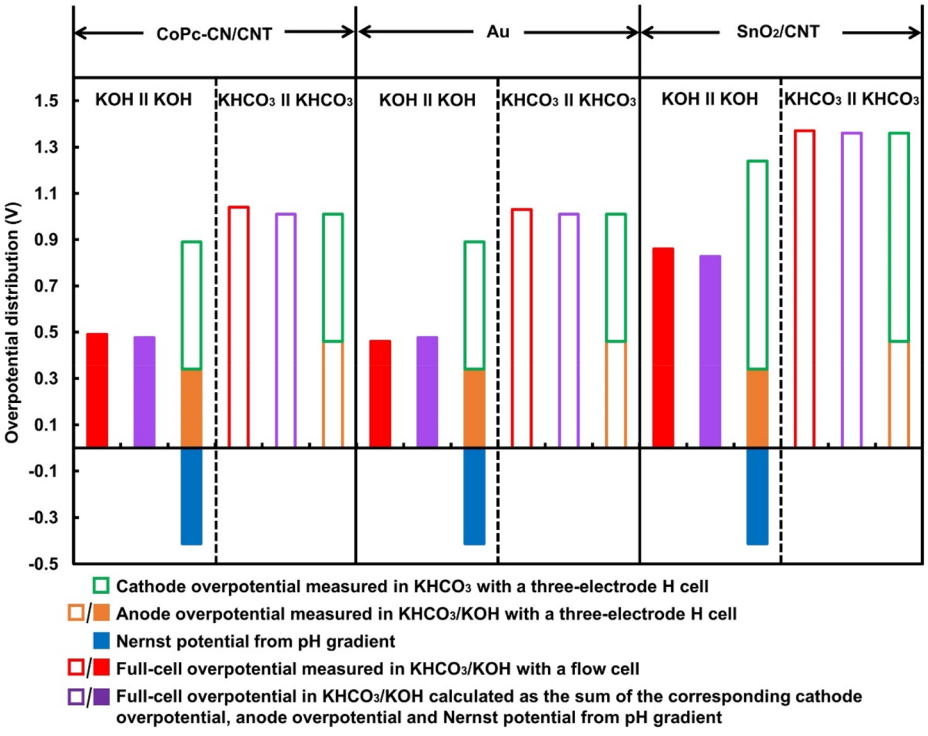

Figure 4. Contributions from cathode overpotential, anode overpotential, and pH gradient to full-cell overpotential for microflow electrolytic cells operating at 20 mA/cm^2 in alkaline or neutral electrolyte with three different cathode catalysts. Good match between the measured and calculated full-cell overpotentials supports our attribution of the overpotential reduction in alkaline electrolyte to the pH gradient and improvement of OER kinetics.

performances with respect to cell voltage, current density, and FE_{CO} (Figures 4, S7, S10, and S11). It should be noted that the dual-electrolyte cell benefits from the Nernst potential between the neutral catholyte and the basic anolyte. Therefore, the KOH cell has at least one more factor other than the OER kinetics that contributes to the overpotential reduction. It could be because of a more efficient CO_2RR in KOH than in $KHCO_3$ or a pH gradient similar to that in the dual-electrolyte cell.

DOI: 10.1021/acsenergylett.8b01681
ACS Energy Lett. 2018, 3, 2527−2532

A previous study explained the cell performance improvement from using KOH electrolyte by assuming a proton-free rate-determining electron-transfer step for the CO_2-to-CO pathway on Au surface,[33] which implies that the CO_2 electroreduction kinetics is faster in more basic electrolyte. This rationale could be consistent with our results on the cells with Au or CoPc-CN/CNT as the cathode catalyst (an overpotential reduction of ∼60 mV per pH unit when switching from KOH to $KHCO_3$ electrolyte), for which the rate-determining step is likely to be non-proton-coupled electron transfer.[43,44] However, it cannot justify the performance of the SnO_2/CNT-based cell, because CO_2 conversion to $HCOO^-$ is a two-electron/one-proton process, for which an assumption of a proton-free rate-determining electron-transfer step would result in a voltage gain of ∼30 mV per pH unit, contradicting our experimental observation. We propose that the existence of a pH gradient is a more suitable explanation to the universal performance improvement of all our KOH cells. Near the cathode surface, a near-neutral layer originates from the chemical reaction between the penetrating CO_2 through the GDE and the KOH electrolyte. Deeper into the bulk where OH^- dominates, the species balance shifts toward a more alkaline environment, creating a pH gradient and introducing a Nernst potential which reduces the overall cell voltage. In combination with the aforementioned pH-dependent OER overpotential which is a relatively minor effect, this can readily explain the overpotential dependence on electrolyte configuration for all our electrolytic cells based on three different cathode catalysts (Figure 4). To verify that CO_2 indeed reacts with KOH at a considerable rate, we monitored the catholyte pH under the electrolyte circulation mode. While electrochemical CO_2RR continues to consume protons, the OH^- was nearly depleted after a 35 h operation (Figure 3c).

In conclusion, we have developed unprecedented electrochemical CO_2RR cells based on non-noble metal catalysts for selective CO and $HCOO^-$ production at low voltages. Electrocatalytic conversion of CO_2 and H_2O to CO or $HCOO^-$ and O_2 onsets at 0.26 and 0.76 V, respectively. High product selectivity, large current density, and good durability are achieved at moderate overpotentials, rivaling the most up-to-date electrolytic CO_2RR devices and approaching technological viability. The superior device performance is a combined result of good catalysts and cell design. This device is potentially suitable for a wide spectrum of catalysts, for instance Cu, which can produce higher-order products such as ethylene and ethanol.

■ ASSOCIATED CONTENT

Supporting Information

The Supporting Information is available free of charge on the ACS Publications website at DOI: 10.1021/acsenergylett.8b01681.

Experimental methods and additional structural and electrochemical characterization results (PDF)

■ AUTHOR INFORMATION

Corresponding Author

*E-mail: hailiang.wang@yale.edu.

ORCID

Zishan Wu: 0000-0003-4810-9112

Hailiang Wang: 0000-0003-4409-2034

Author Contributions

[▽]X. Lu and Y. Wu contributed equally to this work

Notes

The authors declare no competing financial interest.

■ ACKNOWLEDGMENTS

This research is supported by the National Science Foundation (Grant CHE-1651717) and the Croucher Fellowship for Postdoctoral Research. X.Y. and L.H. acknowledge the visiting graduate student scholarships from China scholarships Council.

■ REFERENCES

(1) Qiao, J.; Liu, Y.; Hong, F.; Zhang, J. A Review of Catalysts for the Electroreduction of Carbon Dioxide to Produce Low-Carbon Fuels. *Chem. Soc. Rev.* **2014**, *43*, 631−675.

(2) Zhang, L.; Zhao, Z. J.; Gong, J. Nanostructured Materials for Heterogeneous Electrocatalytic CO_2 Reduction and Their Related Reaction Mechanisms. *Angew. Chem., Int. Ed.* **2017**, *56*, 11326−11353.

(3) Seh, Z. W.; Kibsgaard, J.; Dickens, C. F.; Chorkendorff, I.; Nørskov, J. K.; Jaramillo, T. F. Combining Theory and Experiment in Electrocatalysis: Insights into Materials Design. *Science* **2017**, *355*, eaad4998.

(4) Spurgeon, J. M.; Kumar, B. A Comparative Technoeconomic Analysis of Pathways for Commercial Electrochemical CO_2 Reduction to Liquid Products. *Energy Environ. Sci.* **2018**, *11*, 1536−1551.

(5) Hori, Y.; Kikuchi, K.; Suzuki, S. Production of CO and CH_4 in Electrochemical Reduction of CO_2 at Metal Electrodes in Aqueous Hydrogencarbonate Solution. *Chem. Lett.* **1985**, *14*, 1695−1698.

(6) Fang, Y.; Flake, J. C. Electrochemical Reduction of CO_2 at Functionalized Au Electrodes. *J. Am. Chem. Soc.* **2017**, *139*, 3399−3405.

(7) Zhao, S.; Jin, R.; Jin, R. Opportunities and Challenges in CO_2 Reduction by Gold and Silver-Based Electrocatalysts: From Bulk Metals to Nanoparticles and Atomically Precise Nanoclusters. *ACS Energy Letters* **2018**, *3*, 452−462.

(8) Min, X.; Kanan, M. W. Pd-Catalyzed Electrohydrogenation of Carbon Dioxide to Formate: High Mass Activity at Low Overpotential and Identification of the Deactivation Pathway. *J. Am. Chem. Soc.* **2015**, *137*, 4701−4708.

(9) Gao, D.; Zhou, H.; Cai, F.; Wang, D.; Hu, Y.; Jiang, B.; Cai, W. B.; Chen, X.; Si, R.; Yang, F.; et al. Switchable CO_2 Electroreduction Via Engineering Active Phases of Pd Nanoparticles. *Nano Res.* **2017**, *10*, 2181−2191.

(10) Cao, L.; Raciti, D.; Li, C.; Livi, K. J.; Rottmann, P. F.; Hemker, K. J.; Mueller, T.; Wang, C. Mechanistic Insights for Low-Overpotential Electroreduction of CO_2 to CO on Copper Nanowires. *ACS Catal.* **2017**, *7*, 8578−8587.

(11) Li, Y.; Cui, F.; Ross, M. B.; Kim, D.; Sun, Y.; Yang, P. Structure-Sensitive CO_2 Electroreduction to Hydrocarbons on Ultrathin 5-Fold Twinned Copper Nanowires. *Nano Lett.* **2017**, *17*, 1312−1317.

(12) Weng, Z.; Wu, Y.; Wang, M.; Jiang, J.; Yang, K.; Huo, S.; Wang, X. F.; Ma, Q.; Brudvig, G. W.; Batista, V. S. Active Sites of Copper-Complex Catalytic Materials for Electrochemical Carbon Dioxide Reduction. *Nat. Commun.* **2018**, *9*, 415.

(13) Reller, C.; Krause, R.; Volkova, E.; Schmid, B.; Neubauer, S.; Rucki, A.; Schuster, M.; Schmid, G. Selective Electroreduction of CO_2 toward Ethylene on Nano Dendritic Copper Catalysts at High Current Density. *Adv. Energy Mater.* **2017**, *7*, 1602114.

(14) Mistry, H.; Varela, A. S.; Bonifacio, C. S.; Zegkinoglou, I.; Sinev, I.; Choi, Y. W.; Kisslinger, K.; Stach, E. A.; Yang, J. C.; Strasser, P. Highly Selective Plasma-Activated Copper Catalysts for Carbon Dioxide Reduction to Ethylene. *Nat. Commun.* **2016**, *7*, 12123.

(15) Shinagawa, T.; Larrazábal, G. O.; Martín, A. J.; Krumeich, F.; Perez Ramirez, J. Sulfur-Modified Copper Catalysts for the Electrochemical Reduction of Carbon Dioxide to Formate. *ACS Catal.* **2018**, *8*, 837−844.

DOI: 10.1021/acsenergylett.8b01681
ACS Energy Lett. 2018, 3, 2527−2532

(16) Weng, Z.; Jiang, J.; Wu, Y.; Wu, Z.; Guo, X.; Materna, K. L.; Liu, W.; Batista, V. S.; Brudvig, G. W.; Wang, H. Electrochemical CO_2 Reduction to Hydrocarbons on a Heterogeneous Molecular Cu Catalyst in Aqueous Solution. *J. Am. Chem. Soc.* **2016**, *138*, 8076−8079.
(17) Weng, Z.; Zhang, X.; Wu, Y.; Huo, S.; Jiang, J.; Liu, W.; He, G.; Liang, Y.; Wang, H. Self-Cleaning Catalyst Electrodes for Stabilized CO_2 Reduction to Hydrocarbons. *Angew. Chem., Int. Ed.* **2017**, *56*, 13135−13139.
(18) Zhang, S.; Kang, P.; Meyer, T. J. Nanostructured Tin Catalysts for Selective Electrochemical Reduction of Carbon Dioxide to Formate. *J. Am. Chem. Soc.* **2014**, *136*, 1734−1737.
(19) Li, Q.; Fu, J.; Zhu, W.; Chen, Z.; Shen, B.; Wu, L.; Xi, Z.; Wang, T.; Lu, G.; Zhu, J.; et al. Tuning Sn-Catalysis for Electrochemical Reduction of CO_2 to CO Via the Core/Shell Cu/SnO_2 Structure. *J. Am. Chem. Soc.* **2017**, *139*, 4290−4293.
(20) Huo, S.; Weng, Z.; Wu, Z.; Zhong, Y.; Wu, Y.; Fang, J.; Wang, H. Coupled Metal/Oxide Catalysts with Tunable Product Selectivity for Electrocatalytic CO_2 Reduction. *ACS Appl. Mater. Interfaces* **2017**, *9*, 28519−28526.
(21) Luc, W.; Collins, C.; Wang, S.; Xin, H.; He, K.; Kang, Y.; Jiao, F. Ag-Sn Bimetallic Catalyst with a Core-Shell Structure for CO_2 Reduction. *J. Am. Chem. Soc.* **2017**, *139*, 1885−1893.
(22) Zhang, X.; Wu, Z.; Zhang, X.; Li, L.; Li, Y.; Xu, H.; Li, X.; Yu, X.; Zhang, Z.; Liang, Y.; et al. Highly Selective and Active CO_2 Reduction Electrocatalysts Based on Cobalt Phthalocyanine/Carbon Nanotube Hybrid Structures. *Nat. Commun.* **2017**, *8*, 14675.
(23) Morlanés, N.; Takanabe, K.; Rodionov, V. Simultaneous Reduction of CO_2 and Splitting of H_2O by a Single Immobilized Cobalt Phthalocyanine Electrocatalyst. *ACS Catal.* **2016**, *6*, 3092−3095.
(24) Tatin, A.; Comminges, C.; Kokoh, B.; Costentin, C.; Robert, M.; Savéant, J. M. Efficient Electrolyzer for CO_2 Splitting in Neutral Water Using Earth-Abundant Materials. *Proc. Natl. Acad. Sci. U. S. A.* **2016**, *113*, 5526−5529.
(25) Clark, E. L.; Resasco, J.; Landers, A.; Lin, J.; Chung, L. T.; Walton, A.; Hahn, C.; Jaramillo, T. F.; Bell, A. T. Standards and Protocols for Data Acquisition and Reporting for Studies of the Electrochemical Reduction of Carbon Dioxide. *ACS Catal.* **2018**, *8*, 6560−6570.
(26) Narayanan, S.; Haines, B.; Soler, J.; Valdez, T. Electrochemical Conversion of Carbon Dioxide to Formate in Alkaline Polymer Electrolyte Membrane Cells. *J. Electrochem. Soc.* **2011**, *158*, A167−A173.
(27) Delacourt, C.; Ridgway, P. L.; Kerr, J. B.; Newman, J. Design of an Electrochemical Cell Making Syngas ($CO+H_2$) from CO_2 and H_2O Reduction at Room Temperature. *J. Electrochem. Soc.* **2008**, *155*, B42−B49.
(28) Xu, W.; Scott, K. The Effects of Ionomer Content on Pem Water Electrolyser Membrane Electrode Assembly Performance. *Int. J. Hydrogen Energy* **2010**, *35*, 12029−12037.
(29) Verma, S.; Lu, X.; Ma, S.; Masel, R. I.; Kenis, P. J. The Effect of Electrolyte Composition on the Electroreduction of CO_2 to CO on Ag Based Gas Diffusion Electrodes. *Phys. Chem. Chem. Phys.* **2016**, *18*, 7075−7084.
(30) Ma, S.; Liu, J.; Sasaki, K.; Lyth, S. M.; Kenis, P. J. Carbon Foam Decorated with Silver Nanoparticles for Electrochemical CO_2 Conversion. *Energy Technology* **2017**, *5*, 861−863.
(31) Hoang, T. T.; Verma, S.; Ma, S.; Fister, T. T.; Timoshenko, J.; Frenkel, A. I.; Kenis, P. J.; Gewirth, A. A. Nano Porous Copper-Silver Alloys by Additive-Controlled Electro-Deposition for the Selective Electroreduction of CO_2 to Ethylene and Ethanol. *J. Am. Chem. Soc.* **2018**, *140*, 5791−5797.
(32) Seifitokaldani, A.; Gabardo, C. M.; Burdyny, T.; Dinh, C. T.; Edwards, J. P.; Kibria, M. G.; Bushuyev, O. S.; Kelley, S. O.; Sinton, D.; Sargent, E. H. Hydronium-Induced Switching between CO_2 Electroreduction Pathways. *J. Am. Chem. Soc.* **2018**, *140*, 3833−3837.
(33) Verma, S.; Hamasaki, Y.; Kim, C.; Huang, W.; Lu, S.; Jhong, H. R. M.; Gewirth, A. A.; Fujigaya, T.; Nakashima, N.; Kenis, P. J. Insights into the Low Overpotential Electroreduction of CO_2 to CO on a Supported Gold Catalyst in an Alkaline Flow Electrolyzer. *ACS Energy Letters* **2018**, *3*, 193−198.
(34) Resasco, J.; Chen, L. D.; Clark, E.; Tsai, C.; Hahn, C.; Jaramillo, T. F.; Chan, K.; Bell, A. T. Promoter Effects of Alkali Metal Cations on the Electrochemical Reduction of Carbon Dioxide. *J. Am. Chem. Soc.* **2017**, *139*, 11277−11287.
(35) Chen, L. D.; Urushihara, M.; Chan, K.; Nørskov, J. K. Electric Field Effects in Electrochemical CO_2 Reduction. *ACS Catal.* **2016**, *6*, 7133−7139.
(36) Resasco, J.; Lum, Y.; Clark, E.; Zeledon, J. Z.; Bell, A. T. Effects of Anion Identity and Concentration on Electrochemical Reduction of CO_2. *ChemElectroChem* **2018**, *5*, 1064−1072.
(37) Agarwal, A. S.; Zhai, Y.; Hill, D.; Sridhar, N. The Electrochemical Reduction of Carbon Dioxide to Formate/Formic Acid: Engineering and Economic Feasibility. *ChemSusChem* **2011**, *4*, 1301−1310.
(38) Alvarez Guerra, M.; Del Castillo, A.; Irabien, A. Continuous Electrochemical Reduction of Carbon Dioxide into Formate Using a Tin Cathode: Comparison with Lead Cathode. *Chem. Eng. Res. Des.* **2014**, *92*, 692−701.
(39) Jones, J. P.; Prakash, G.; Olah, G. A. Electrochemical CO_2 Reduction: Recent Advances and Current Trends. *Isr. J. Chem.* **2014**, *54*, 1451−1466.
(40) Whipple, D. T.; Finke, E. C.; Kenis, P. J. Microfluidic Reactor for the Electrochemical Reduction of Carbon Dioxide: The Effect of pH. *Electrochem. Solid-State Lett.* **2010**, *13*, B109−B111.
(41) Gerken, J. B.; McAlpin, J. G.; Chen, J. Y.; Rigsby, M. L.; Casey, W. H.; Britt, R. D.; Stahl, S. S. Electrochemical Water Oxidation with Cobalt-Based Electrocatalysts from pH 0−14: The Thermodynamic Basis for Catalyst Structure, Stability, and Activity. *J. Am. Chem. Soc.* **2011**, *133*, 14431−14442.
(42) Zhao, Y.; Chen, S.; Sun, B.; Su, D.; Huang, X.; Liu, H.; Yan, Y.; Sun, K.; Wang, G. Graphene-Co_3O_4 Nanocomposite as Electrocatalyst with High Performance for Oxygen Evolution Reaction. *Sci. Rep.* **2015**, *5*, 7629.
(43) Varela, A. S.; Kroschel, M.; Leonard, N. D.; Ju, W.; Steinberg, J.; Bagger, A.; Rossmeisl, J.; Strasser, P. pH Effects on the Selectivity of the Electrocatalytic CO_2 Reduction on Graphene-Embedded Fe-N-C Motifs: Bridging Concepts between Molecular Homogeneous and Solid-State Heterogeneous Catalysis. *ACS Energy Letters* **2018**, *3*, 812−817.
(44) Chen, Y.; Li, C. W.; Kanan, M. W. Aqueous CO_2 Reduction at Very Low Overpotential on Oxide-Derived Au Nanoparticles. *J. Am. Chem. Soc.* **2012**, *134*, 19969−19972.

DOI: 10.1021/acsenergylett.8b01681
ACS Energy Lett. 2018, 3, 2527−2532